Regional Ventilation Is the Main Determinant of Alveolar Deposition of Coarse Particles in the Supine Healthy Human Lung During Tidal Breathing

Rui Carlos Sá, PhD,[1] Kirby L. Zeman, PhD,[2] William D. Bennett, PhD,[2] G. Kim Prisk, PhD, DSc,[1,3] and Chantal Darquenne, PhD[1]

Abstract

Background: To quantify the relationship between regional lung ventilation and coarse aerosol deposition in the supine healthy human lung, we used oxygen-enhanced magnetic resonance imaging and planar gamma scintigraphy in seven subjects.

Methods: Regional ventilation was measured in the supine posture in a 15 mm sagittal slice of the right lung. Deposition was measured by using planar gamma scintigraphy (coronal scans, 40 cm FOV) immediately postdeposition, 1 hour 30 minutes and 22 hours after deposition of ^{99m}Tc-labeled particles (4.9 μm MMAD, GSD 2.5), inhaled in the supine posture (flow 0.5 L/s, 15 breaths/min). The distribution of retained particles at different times was used to infer deposition in different airway regions, with 22 hours representing alveolar deposition. The fraction of total slice ventilation per quartile of lung height from the lung apex to the dome of the diaphragm at functional residual capacity was computed, and co-registered with deposition data—apices aligned—using a transmission scan as reference. The ratio of fractional alveolar deposition to fractional ventilation of each quartile (r) was used to evaluate ventilation and deposition matching ($r > 1$, regional aerosol deposition fraction larger than regional ventilation fraction).

Results: r was not significantly different from 1 for all regions (1.04 ± 0.25, 1.08 ± 0.22, 1.03 ± 0.17, 0.92 ± 0.13, apex to diaphragm, $p > 0.40$) at the alveolar level (r_{22h}). For retention times r_{0h} and r_{1h30}, only the diaphragmatic region at r_{1h30} differed significantly from 1.

Conclusions: These results support the hypothesis that alveolar deposition is directly proportional to ventilation for $\sim 5 \mu$m particles that are inhaled in the supine posture and are consistent with previous simulation predictions that show that convective flow is the main determinant of aerosol transport to the lung periphery.

Keywords: coarse aerosol deposition, human lung, multimodal imaging, ventilation

Introduction

INHALED DRUGS ARE AN IMPORTANT PART of addressing respiratory disease, as inhalation presents the advantage of a lower, more targeted dose to lung tissues, thus limiting undesired side effects, and also providing rapid action compared with oral administration routes.[1] Inhaled medication is the primary administration route for many drugs in asthma and chronic obstructive pulmonary disease, and it is also extensively used in treating cystic-fibrosis.

Many factors affect the distribution of inhaled particles in the human lung. Some are controllable, such as particle size,[1–4] inspiratory flow,[5] breath hold duration,[6,7] and inhalation posture,[8] whereas others are less so, such as individual airway geometry[9] and localized heterogeneous constriction.[10,11]

Targeted delivery of inhaled drugs, directly addressing the underlying pathology, is an active research field with the potential to enhance clinical outcomes.[12] For example, bronchodilators maximize their effect by targeting receptors in the smooth muscle in conducting airways,[5] whereas

[1]Pulmonary Imaging Laboratory, Department of Medicine, University of California, San Diego, La Jolla, California.
[2]Department of Medicine, University of North Carolina at Chapel Hill, Chapel Hill, North Carolina.
[3]Pulmonary Imaging Laboratory, Department of Radiology, University of California, San Diego, La Jolla, California.

corticosteroids are believed to have greater benefit by topical action[13] with receptors present in large, intermediate, and small airways.[14] On the other hand, systemic targeting of drugs by aerosol administration intended for other organs, for example, aerosolized vaccination and insulin, benefits from targeted delivery to the lung periphery.[15,16]

Typical particle size in inhaled medication ranges from 1 to 5 μm.[5] The range is a compromise between smaller particles that penetrate deeper into the lung, but require longer breath holds to deposit (otherwise, they tend to remain in suspension and to be subsequently exhaled),[2] and larger particles that mostly deposit in the upper airways[1] through impaction. It is generally accepted that aerosolized drugs reach the small airways and the alveolar lung region in direct proportion to regional flow.[17] Computational fluid dynamics simulations in realistic human airway geometries support the notion that this proportionality to convective flow is the main determinant of aerosol delivery all the way to sublobar lung segments[17] for particles that are smaller than 10 μm. However, these studies lack experimental verification.

Previous experimental work relating regional deposition and regional alveolar ventilation in the human lung is, to the best of our knowledge, limited, and has provided conflicting results: Using planar gamma scintigraphy, Brown et al.[18] have shown a significant linear association between regional deposition and regional ventilation both in healthy and in CF subjects in the seated posture; in a different population (HIV) and using smaller particles (<2.5 μm), O'Riordan and Smaldone[19] reached the opposite conclusion.

The goal of this study was to quantify the relationship between regional lung ventilation and aerosol deposition in the healthy human, testing the hypothesis that for 5 μm particles the regional alveolar deposition is proportional to regional ventilation.

We used two imaging modalities, gamma scintigraphy and functional magnetic resonance imaging (MRI), to quantify particle deposition and ventilation in the same subjects, respectively.

Relative deposition throughout the lung was acquired by using planar gamma scintigraphy, using [99mTc]-labeled aerosolized particles, with particle inhalation taking place in the supine posture. The retention time course over 22 hours after aerosol inhalation was used to associate deposition to different components of the airway tree, that is, large airways, and the alveolar region, based on how quickly clearance occurred.[7,18,20–22] Basically, particles depositing in the large airways are cleared faster by mucociliary transport than particles depositing in the lung periphery where mucociliary transport is not present. In particular, particles that are cleared in the first 1 hour 30 minutes are associated with large airways,[23,24] whereas particles remaining at 22 hours represent alveolar lung region deposition.[25,26]

In the same subjects and for the same posture, we used MRI to quantify ventilation in a representative slice of the right lung. The combined analysis of deposition and ventilation maps allowed us to compute the ratio of regional deposition fraction to regional ventilation.

Methods

Subjects

This study was approved by the Human Subjects Research Protection program at the University of California, San Diego, and by the Committee on the Protection of the Rights of Human Subjects at the University of North Carolina, Chapel Hill. Subjects participated after giving written informed consent. We acquired complete datasets in seven subjects (four women, three men). All subjects were between the ages of 26 and 59, were nonsmokers, had no history of bronchial reactivity, and had normal pulmonary function as measured by spirometry (FEV$_1$ and FEV$_1$/FVC: 98% ± 11% and 104% ± 6% predicted, respectively). Table 1 presents a summary of subject characteristics and main pulmonary function data.

We mapped the deposition of particles inhaled in the supine posture (gamma scintigraphy), and we compared it with the distribution of ventilation (MRI), also acquired in the supine posture, in the same healthy subjects. For all subjects, particle deposition data were acquired first at the University of North Carolina, Chapel Hill, and MRI ventilation data were acquired later at the University of California, San Diego (on average, 110 days between studies).

Gamma scintigraphy

We used planar gamma scintigraphy to map the deposition and subsequent clearance of ~5 μm [99mTc]-labeled particles, with particles inhaled in the supine posture. Deposition data for six of the subjects presented in this article were previously reported in a study comparing supine and upright deposition and clearance[8]; for consistency, we have maintained the same subject numbering.

Aerosol generation and inhalation

We used [99mTc]-sulfur colloid particles (10 mCi/370 MBq), prepared from CIS-Sulfur colloid kits (CIS-US, Inc., Bedford, MA), with a mean diameter of 0.22 μm (geometric standard deviation 1.75), suspended into normal (0.9%) saline. The solution was nebulized by using a vibrating mesh nebulizer

TABLE 1. ANTHROPOMETRIC AND RESPIRATORY FUNCTION DATA

Subject no	Gender	Age(year)	Height(cm)	Weight (kg)	FEV$_1$ (L)	FEV$_1$ (% pred)	FEV$_1$/FVC	FEV$_1$/FVC (% pred)
1	F	44	165	57	3.16	104	0.78	96
2	F	39	162	66	3.03	101	0.83	101
4	M	54	186	120	4.28	101	0.88	114
8	F	47	173	83	2.76	83	0.89	110
9	F	26	174	95	3.49	95	0.86	101
10	M	36	178	85	3.69	85	0.81	101
11	M	59	178	70	4.25	116	0.79	104
		44 ± 11	174 ± 8	82 ± 21	3.52 ± 0.59	98 ± 11	0.83 ± 0.04	104 ± 6

(Aeroneb Laboratories, Nektar, San Carlos, CA) for inhalation. As in previous studies,[8,20] the nebulizer was in series with the breathing path, and it was lead-shielded; room contamination from exhaled particles was prevented by placing a filter on the distal end of the circuit. The circuit design minimized the deadspace between the nebulizer and the mouthpiece, to avoid evaporation before inhalation. The generated droplet size was $4.9\,\mu m$ (MMAD) with a geometric standard deviation of 2.5, as measured by an eight-stage cascade impactor (Sierra Instruments, Carmel Valley, CA).

Particle inhalation was done at a target flow of 0.5 L/s, for 2 seconds (1 L tidal breathing, at 15 breaths/min), with the timing cues provided by a metronome, and real-time visual feedback of respiratory flow. Subjects were in the supine posture, mouth breathing and using a nose clip, lying on top of a gamma camera. The target deposited dose was $40\,\mu Ci$, and particle inhalation was stopped when the target (above background) was reached. This required on average 14 breaths.

The same single-head gamma scintigraphy camera was used for all image acquisition presented in this article; a different gamma camera compatible with supine imaging was used solely for initial dose determination. After the initial deposition in the supine posture, subsequent gamma scintigraphy data were acquired in the seated posture. When not being scanned, subjects were free to pursue normal activities; subjects were asked to refrain from exercise for the ~ 24 hour duration of the study.

Gamma scintigraphy imaging

Images were acquired by using a 40 cm single-head gamma scintigraphy camera (Orbiter; MiE America, Chicago, IL), fitted with a parallel-hole collimator. Similar to our previous study,[8] data acquisition was performed immediately postexposure ($t = 0$ hour), 1 hour 30 minutes and 22 hours postparticle deposition. Static images were acquired over 10 minutes immediately postexposure, over 15 minutes at $t = 1$ hour 30 minutes and over 30 minutes at $t = 22$ hours. At all time points, scans were performed in the seated posture, with the subject free to breathe normally (tidal breaths) throughout the acquisition. Two point sources (Americium-241, $<1\,\mu Ci$) placed on the subject's back in marked locations along the spine, but outside the lung field, were used as fiduciary markers, to control for changes in subject placement between acquisitions at different times.

Background activity level was measured by acquiring images with the subject in front of the camera before particle inhalation, and stability and uniformity of the camera was checked daily. The lung field for each subject was delineated by using an additional transmission scan (Cobalt-57 planar source, <25 mCi, placed in front of the subject for ~ 90 seconds), before particle inhalation.

Estimating deposition in different anatomical regions of the airway tree

All data reported in this article are associated with the right lung. This avoided the confounding effect of stomach activity in the gamma scintigraphy data at $t = 0$ hour. Using the ^{57}Co transmission scan image, a region of interest (ROI) selecting the right lung was drawn. This ROI was used to co-register the ventilation and deposition data, as explained next.

As in previous studies, the retention at different times (R_t), defined as the half-life corrected fraction of remaining activity at each time t, was used to assign deposition to different regions of the airway tree. Assuming negligible alveolar clearance in the 22 hours immediately postdeposition and complete clearance of the large ciliated airways in the same period,[25,27–30] alveolar deposition was estimated by the retention at $t = 22$ hours (R_{22h}). Under similar assumptions of clearance times in the large ciliated airways,[23] R_{1h30} integrated both alveolar deposition and particles deposited in the intermediate and small bronchial airways, and the R_{0h} integrated the entire airway tree, including the large airways.

Magnetic resonance imaging

To quantify ventilation, two different proton MR sequences were used, a multi-echo fast gradient (mGRE) sequence to quantify lung density,[31,32] and specific ventilation imaging,[33,34] an oxygen-enhanced proton MRI technique that was capable of quantifying specific ventilation (the ratio of fresh gas delivered to a lung region to the region's gas volume at functional residual capacity [FRC]). Both were acquired in a single ~ 30 minute session, using a 1.5-T EXCITE HDx TwinSpeed MRI system (General Electric Medical Systems, Milwaukee, MI). For the estimation of lung density, acquisition followed the work presented in Ref. [31] and specific ventilation imaging was performed as described in Ref. [33] by using the data analysis approach described in Ref. [34] For completeness, these techniques are briefly presented next.

Both techniques quantified a 15 mm sagittal lung slice, acquired in the right lung. The selected slice was located in the mid-clavicular line, and chosen to present the largest superior-inferior dimension, while avoiding major hilar vessels. All MR images were acquired at FRC, either during a ~ 9 second breath hold (density) or in a series of ~ 1 second end-expiratory breathing pauses at the end of regular breaths (specific ventilation). The pace of breathing was imposed (1 breath every 5 seconds, 12 breaths/min), whereas subjects were free to adopt a natural tidal volume (unconstrained tidal volume); the breathing pattern was measured (see "Specific ventilation imaging" section below).

The subject lay supine in the MRI scanner, wearing a facemask (Hans Rudolph, KS, depending on mask size, deadspace 73–113 mL) attached to a nonrebreathing T-valve (28 mL deadspace; Hans Rudolph), with the inspiratory port connected to a remote-controlled three-way pneumatic valve (model 8500; Hans Rudolph). The valve allowed rapid switching of inspired gas concentration, as required by the specific ventilation protocol. The inspiratory resistance between both inspiratory paths (air and oxygen) was matched to avoid changes in FRC created by different inspiratory impedances. The expiratory side was connected to a large bore, low resistance tube, leading outside of the scanner, where tidal volume, expired gas concentration, and other respiratory variables were measured (ParvoMedics, Sandy, UT).

Lung density.   Lung density at end expiration (FRC) was acquired by using an mGRE sequence, described in detail in Ref. [31] In short, 12 images were acquired at two alternating echo times (1.1 and 1.8 msec), during a ~ 9 second breath hold. Proton density was estimated by back extrapolating the signal to an echo time of 0, assuming a

mono-exponential decay. The first two images at each echo time were discarded, and only the steady-state data were used. Absolute quantification was obtained by comparison with a reference phantom, of known properties.

This technique was validated against gravimetric measurement of excised pig lungs,[32] and repeated measurements proved excellent reliability.[32] Scanner parameters for this acquisition were as follows: $TR = 10$ msec, flip angle: $10°$, slice thickness $= 15$ mm, field of view $= 40 \times 40$ cm (typically), receiver bandwidth $= 125$ kHz, and acquisition matrix: 64×64. The back extrapolated quantitative density was expressed as: (mL of (water+blood)/cm^3).

Specific ventilation imaging

Specific ventilation imaging (SVI) is based on the fact that oxygen is a T_1 contrast agent (increased local oxygen concentration shortens T_1), increasing regional signal intensity in appropriately prepared and acquired MR images. After a sudden change in inspired oxygen concentration, the rate of change of the local O_2 concentration in lung tissue, and thus signal intensity, is determined mainly by the regional specific ventilation—regions with a higher specific ventilation will reach the new equilibrium faster than regions with a lower specific ventilation.

The time course of the regional MR signal intensity was used to quantify specific ventilation, using an inversion recovery sequence, with an inversion time that maximizes the air-oxygen difference. We acquired a series of consecutive two-dimensional T_1-weighted images (inversion recovery, $T_I = 1100$ msec) by using a single-shot fast spin echo sequence, using half Fourier (HASTE) sampling of a 256×128 Fourier space. The field of view was 40×40 cm, with a 15 mm-thick slice. Images were reconstructed to a 256×256 grid (in-plane resolution ~ 1.6 mm, corresponding to a sampling volume ~ 40 mm^3).

Images were acquired 5 seconds apart, at FRC, during a short pause at the end of a normal breath. The first 20 images were acquired with the subject inspiring room air; the next 20 images were acquired with the subject inspiring 100% oxygen. A total of five air-oxygen cycles were acquired consecutively; 20 additional images while inspiring 100% oxygen were added at the end to increase the ability to identify regions of low specific ventilation, resulting in a total of 220 breaths (~ 18 minutes).

Oxygen was delivered by using a prefilled 170-L Douglas bag (Hans Rudolph, type 6170). Subjects were instructed to take regular tidal breaths after each image, as signaled by the scanner sounds, and to relax to FRC before the next image acquisition. Images were acquired with as little disruption to a normal breathing cycle as possible, during a ~ 1 second postexpiratory pause at FRC. Expired tidal volume was measured in parallel.

Quantification of specific ventilation was based on an individualized simulation (subject by subject, based on measured tidal volume) of the temporal response of 50 ideal lung units, subjected to the imposed changes in inspired oxygen concentration. Each ideal unit was assigned a specific ventilation value ranging from 0.01 to 10, which was equally spaced in $\log_{10}$ (unit $n+1$ was assigned a specific ventilation 15% greater than unit n). This generates a library of simulated temporal responses to the alternating air-oxygen stimulus.

The breath-by-breath time series of each voxel inside a user-defined ROI corresponding to the lung was correlated with the library of simulated responses, with the maximum correlation determining the value of specific ventilation assigned to each voxel.[34] The value for specific ventilation was retained only if the maximal correlation was significant ($p < 0.05$) and the null hypothesis (no correlation) was rejected. Voxels where the null hypothesis could not be rejected were treated as missing data. The method and algorithm were validated against nonspatial measurements of specific ventilation heterogeneity.[34]

Before the correlation computation, for each subject, all images in the SVI time series were visually inspected and co-registered to a reference image selected from the time series, using projective deformable image registration at subvoxel scale.[35,36] The deformation algorithm was based on the lung boundary and ignored information in the lung field. When co-registration of a particular image resulted in >10% average area change, the image was removed and replaced by an image constructed from the preceding and following images. All MRI data analysis was performed by using Matlab (Mathworks, Natick, MA).

Combining lung density and specific ventilation maps to quantify ventilation

The density and SVI images were co-registered by using deformable image registration (projective deformation,[36] based on the lung boundary), and smoothed to ~ 1 cm^3 resolution by using a Gaussian kernel low-pass filter, applied in the frequency domain, to minimize potential small misalignments between the two modalities.

To quantify ventilation, we assumed that each voxel is composed of two components, air and tissue, with density 0 and 1. The local water fraction (density D) is, thus, a measure of the fraction of tissue (including blood and other intra/extra-cellular water) in the voxel. As such, to a first approximation, (1-D) is an estimate of the amount of gas in the voxel. A small ($\sim 10\%$) nonproton MR measurable component is present,[37] so the gas fraction in each voxel is more accurately described by (1–1.1 D).

Ventilation in units of mL (fresh gas)/cm^3/min was computed on a voxel-per-voxel basis, as

$$\dot{V} = Resp_{rate} \cdot sV \cdot (1 - 1.1\ D),$$

where $Resp_{rate}$ is the respiratory rate (breaths per minute) and sV is the specific ventilation in the voxel.

Comparing ventilation with particle deposition

The acquired gamma scintigraphy data were a coronal projection of deposition, integrated in the antero-posterio direction over the entire lung field, whereas the ventilation map sampled a sagittal slice of the lung. The first step required to combine these images was to co-register them in the cranio-caudal and medial-lateral directions.

A region of interest (ROI$_{Dep}$), drawn in the gamma scintigraphy transmission scan, was used as a reference. All subsequent deposition images were co-registered to this reference by using the Americium markers as fiducial markers. Since the fiducial markers were not present in the MRI data, medial-lateral alignment of the sagittal MRI data

was assumed to correspond to the 15 mm lung slice immediately lateral to the mid-line of the right lung ROI in the transmission scan (Fig. 1). This approach places the sampled region in the lung periphery, away from the potential confounding effect of large airways and parts of the bronchial tree, which are mostly present in the central region, medial to the selected slice location.[38,39]

For cranial-caudal alignment, the apex of the lung was used as a reference, because this region has minimal movement. The top of the lung slice in the transmission image was defined as the mid-height across the five voxels in the medial-lateral direction. For the ROI drawn in the MRI data (ROI$_{Vent}$), the local lung apex was determined, and the ''tops'' were aligned across modalities.

The distance from the local apex to the local dome of the diaphragm measured from ROI$_{Vent}$ was used to partition the lung in the cranio-caudal direction into 4 equal-height spatial regions, starting from the local apical co-registered points: apical, mid-apical, mid-diaphragmatic, and diaphragmatic. Voxels caudal to the diaphragmatic dome at FRC were discarded from the analysis (in both modalities), as respiratory movements (diaphragmatic displacement) present in the gamma scintigraphy data prevent a direct comparison across modalities. The lung volume of the selected lung slice at FRC for each spatial region was computed by using the MRI data.

The ratio of the regional fraction of deposition to the regional fraction of ventilation (r_t) was computed as

$$r_t = \frac{fraction\ of\ regional\ deposition}{fraction\ of\ regional\ ventilation}\bigg|_t$$

for all regions (apical, mid-apical, mid-diaphragmatic, diaphragmatic), for all airway retention times (r_{22h} corresponding to the alveolar lung region and nonciliated distal spaces, r_{1h30} including alveolar, small, and intermediated airways, and r_{0h} referring to total deposition, including large airways). By construction, this index is 1 when the regional deposition is proportional to the regional ventilation, r_{region} >1 when the regional fractional deposition exceeds the fraction of the regional ventilation, and r_{region} <1 when the fraction of deposition in the region is smaller than the regional ventilation fraction. By choice of the MRI slice location, few, if any, large and intermediate airways were expected to be present, and our main focus was on alveolar deposition.

Statistical analysis

For each subject, spatial and anatomical region, the ratio of the regional fraction of deposition to the regional fraction of ventilation was computed. Wilcoxon signed-rank tests comparing spatial regions (apical, mid-apical, mid-diaphragmatic, and diaphragmatic) and comparing each region with a hypothetical value of 1 were used to compare the regional fraction of deposition with the regional fraction of ventilation across the different regions. The significance level was set at $p < 0.05$. All statistical analyses were performed by using Prism v5.0 (Graphpad, San Diego, CA).

Results

The deposition and ventilation data obtained from this study are depicted in Figure 1. It shows, in the XY plane, a
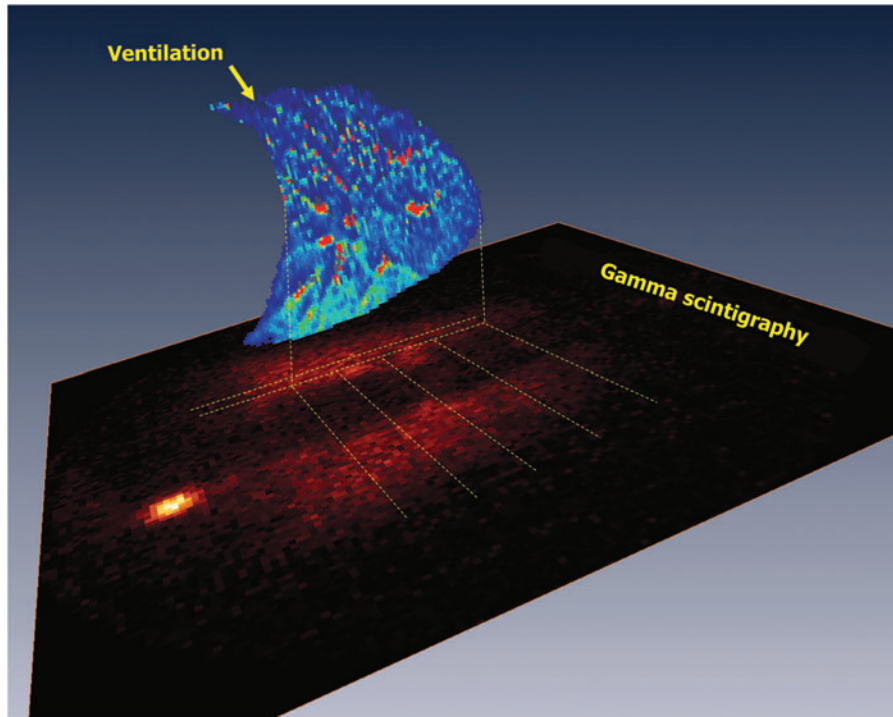

FIG. 1. Gamma scintigraphy acquired deposition scan, with a sagittal map of ventilation of a 15 mm slice of the right lung superimposed. The ventilation in each cranio-caudal quartile was integrated to estimate total ventilation to each region, indicated by the parallel dashed lines. Images were co-registered.
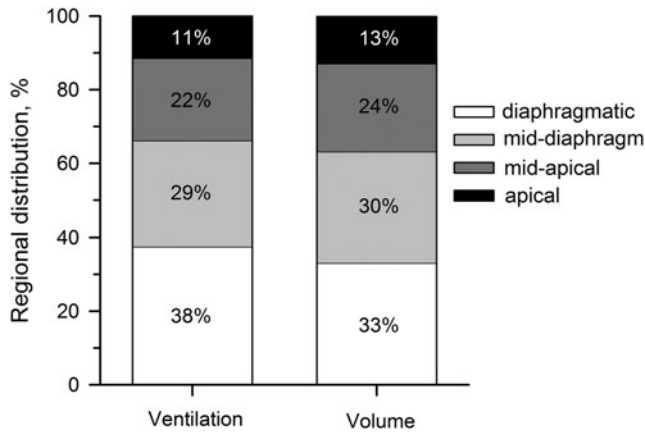
FIG. 2. Fraction of ventilation directed to and the lung volume contained in each of the four regions analyzed.

background-corrected R_{22h} gamma scintigraphy map of an alveolar deposition image, obtained as a coronal projection of deposited particles remaining in the lung 22 hours postdeposition. In the ZX plane, at the corresponding slice location, the sagittal map of ventilation acquired in the same subject is also presented. The apices of the two lung images (MRI, sagittal; gamma scintigraphy, coronal projection) are aligned, as explained in the Methods section, allowing for a direct comparison of regional deposition and ventilation.

Total ventilation per quartile of lung slice, over all subjects ($N = 7$), was distributed as shown in Figure 2: $11.4\% \pm 3.5\%$, $22.4\% \pm 4.6\%$, $28.7\% \pm 1.2\%$, and $37.5\% \pm 7.8\%$ to the apical, mid-apical, mid-diaphragmatic, and diaphragmatic regions, respectively. These regions of the lung corresponded to $12.8\% \pm 1.6\%$, $23.9\% \pm 1.3\%$, $30.1\% \pm 1.3\%$, and $33.1\% \pm 2.2\%$ of imaged volume of the sagittal slice imaged. The ratios of ventilation to lung volume for each quartile were 0.89 ± 0.23 (apical), 0.93 ± 0.16 (mid-apical), 0.95 ± 0.07 (mid-diaphragmatic), and 1.13 ± 0.21 (diaphragmatic). A linear fit to the volume-ventilation curve presented a slope of 1.02 ($R^2 = 0.95$).

Alveolar deposition, as estimated by the fraction of activity remaining 22 hours postinhalation, was partitioned $10.1\% \pm 4.2\%$ to the apical region, $22.2\% \pm 6.9\%$ to the mid-apical region, $31.7\% \pm 5.3\%$ to the mid-diaphragmatic region, and $36.0\% \pm 7.7\%$ to the diaphragmatic region, respectively. This is presented in Table 2, together with the

relative portion of retained particles per region at times $t = 0$ hours and 1 hour 30 minutes.

The ratio of the regional fraction of deposition to the regional fraction of ventilation (r_t), the primary endpoint reported in this study, is presented in Table 3 for all time points, and also in Figure 3 for 22 hours. For r_{22h}, representing the ratio of fractional regional alveolar deposition to regional ventilation, over all regions, this ratio was not different from 1 ($p > 0.40$ for all regions), indicating a one-to-one correspondence between regional deposition and ventilation. For r_{1h30}, where not only alveolar deposition but also deposition in the small and intermediate airways is present, the ratio was not different from 1, except for the diaphragmatic region ($p = 0.01$ for r_{1h30}, all other $p > 0.11$). Even though significantly different from 1, the ratio r remained similar to that representing alveolar deposition alone (diaphragmatic $r_{22h} = 0.92$ and $r_{1h30} = 0.91$). The ratio r_{0h}, representative of deposition in the whole lung immediately after aerosol exposure in the supine position, was not different from 1.

Discussion

In support of our hypothesis, subjects with a normal lung function who tidally inhaled $5 \mu m$ particles in the supine posture had alveolar deposition that was directly proportional to ventilation throughout the lung. This is indicated by the ratio of the regional fraction of deposition to the regional fraction of ventilation, which was not significantly different from 1 for all regions (apical, mid-apical, mid-diaphragmatic, and diaphragmatic) at a retention time of 22 hours.

These results are in accordance with previous simulation predictions from our group, showing that convective flow is the main determinant of aerosol transport to the lung periphery.[17] This previous work used a realistic model of the human airway tree extending from the trachea to the segmental bronchi, in which particle transport was simulated for particle diameters ranging from 0.5 to 10 μm, at different inspired flows (100–500 mL/s). This study introduced the ratio comparing the fraction of particles delivered at the outlet of the model (segmental bronchi) with the distribution of ventilation exiting the model outlet, which, in turn, was the basis of the ratio of the regional fraction of deposition to the regional fraction of ventilation used in the present work.

For somewhat smaller particles (2 μm diameter), Darquenne et al.[17] reported proportionality between regional delivery of particles and regional flow (ratios in the 0.85–1.07 range), and a very small relative dispersion ($\sim 5\%$) of

TABLE 2. RELATIVE DISTRIBUTION OF PARTICLES RETAINED IN THE LUNG SLICE (ROI_{DEP}) AT DIFFERENT TIMES (0 HOUR, 1 HOUR 30 MINUTES, AND 22 HOURS) AND REGIONAL FRACTION OF VENTILATION IN THE SAME LUNG SLICE

	Deposition (%)			
	t = 0 h	*t = 1 h 30 min*	*t = 22 h*	*Ventilation (%)*
Apical	12.8 ± 1.6	13.0 ± 3.7	10.1 ± 4.2	11.4 ± 3.5
Mid-apical	23.4 ± 2.2	24.0 ± 2.4	22.2 ± 6.9	22.4 ± 4.6
Mid-diaphragm	30.0 ± 1.6	29.9 ± 1.8	31.7 ± 5.3	28.7 ± 1.2
Diaphragmatic	33.9 ± 3.7	33.1 ± 5.1	36.0 ± 7.7	37.5 ± 7.8

Data are averaged over seven subjects (mean ± SD).
ROI, region of interest.

	Apical	Mid-apical	Mid-diaphragm	Diaphragmatic
r_{0h}	1.07 ± 0.22	1.01 ± 0.12	1.02 ± 0.06	0.97 ± 0.08
r_{1h30}	1.16 ± 0.25	1.04 ± 0.13	1.03 ± 0.08	0.91 ± 0.07[a]
r_{22h}	1.04 ± 0.25	$1.08 \pm 0.0.22$	1.03 ± 0.17	0.92 ± 0.13

[a]Statistical significance ($p < 0.05$) from $r_t = 1.0$.

this ratio across the lung segments, independent of inspired flow. By depositing the particles and imaging ventilation in the supine posture, we minimized the relative importance of gravity, and we focused on the importance of airway geometry. Together, the present experimental results on particle deposition in the healthy lung and the outcomes of simulations on particle transport to the periphery support the findings that the spatial heterogeneity of ventilation distribution resulting either from inter-individual differences and/or from disease is a main determinant of aerosol targeting of inhaled medication to the lung periphery.

Given the location of the sagittal lung slice selected for the ventilation portion of this study, most of the lungs sampled correspond to the alveolar region, potentially containing small airways, but likely few intermediate airways, and fewer, if any, large airways. Therefore, we expected no change between the indices for r_{0h} and r_{1h30} compared with r_{22h}. A two-way Anova analysis with time and lung region as factors indicated a significant effect of lung region ($p = 0.02$), but not time ($p = 0.89$) or interaction ($p = 0.76$), as expected.

Despite the statistically significant difference from 1 observed for r_{1h30} in the diaphragmatic region, the difference is physiologically insignificant, given that the ratio varied only between 0.91 and 0.92. Moreover, the diaphragmatic region results in the least reliable data in both techniques: Free breathing during gamma scintigraphy acquisition, although addressed partially by cropping the ROI at the diaphragmatic dome height at FRC, makes the deposition estimation of this region less reliable. Ventilation imaging

FIG. 3. Ratio of fractional regional deposition to fractional regional ventilation, for r_{22h}. Individual (symbols) and averaged (mean ± SD) data are shown.

involves taking 220 consecutive images of the lung at FRC: Small variations of the diaphragmatic position were either corrected for by using image registration (for small displacements) or excluded (for large displacements), and spatial smoothing was applied to minimize effects of small remaining mis-registration; however, this region remains the most prone to quantification errors for ventilation.

Previous literature comparing regional deposition and regional alveolar ventilation is, to the best of our knowledge, limited. The most comparable prior study, by Brown et al.,[18] studied the relationship between regional deposition of coarse particles and regional ventilation, using planar gamma scintigraphy and similar-sized particles. Deposition was quantified by using ^{99m}Tc-labeled monodisperse particles (4.9 μm MMAD), imaged immediately postdeposition and 24 hours later; ventilation was quantified by using equilibrium and washout ^{133}Xe scans.

Our results are in accordance with the positive linear association between regional deposition and ventilation reported for 11 healthy subjects.[18] The three main differences between the two studies are: (1) the use of monodisperse (GSD <1.2) vs. polydisperse particles (here GSD = 2.5); (2) ^{133}Xe washout in Brown et al. vs. MRI for regional ventilation quantification; and, most importantly, (3) the difference in posture (seated in Brown et al., supine here), which allows us to minimize the effect of gravity on regional ventilation, and, thus, brings forward the effects of nongravitational differences (lung anatomy, structure, branching angles of the airway tree).

Brown et al.[18] reported an apex to basal (gravitational direction) gradient on regional ventilation and regional particle deposition, that is, by construction, minimized or absent from our analysis. By minimizing the gravitational lung deformation (supine posture) and integrating it into the gravitational axis, our study focused on the intrinsic, nongravitational-induced differences present in the lung (anatomy, structure, branching angles of the airway tree) and the regional variability in function (regional differences in ventilation). Our results, using an independent and a very different measure of ventilation than that used by Brown et al., support the proportionality of regional deposition to regional ventilation at the lobar scale.

In addition to the different posture and ventilation measurement technique, this study and the study by Brown et al. differed on the inhaled particle distribution (similar MMAD, yet monodisperse versus polydisperse, GSD = 2.5). The contribution of particles that are significantly larger than 5 μm to the measured regional alveolar deposition is likely small, as they will preferentially deposit in the upper airways by inertial impaction, thus representing a small fraction of the total deposition measured in the alveolar region at the selected slice location; particles that are significantly
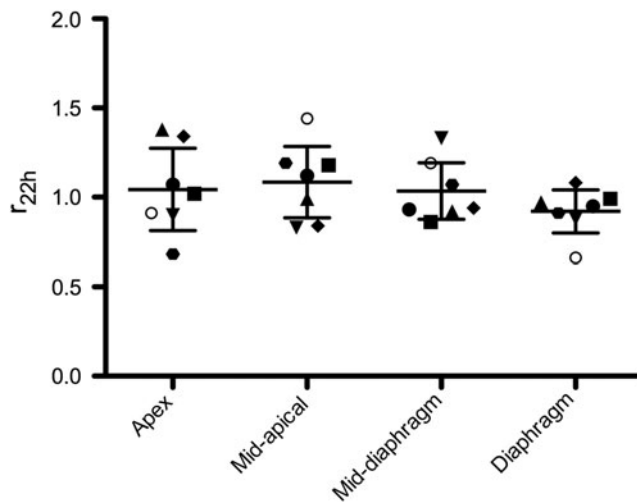
smaller than 5 μm will likely penetrate deeper into the lung periphery, where most will deposit (some may remain in suspension and be exhaled), yet are unlikely to influence the overall conclusion of the study.

Using inhaled krypton-81 m to measure ventilation and technetium-99 m-labeled particles to measure aerosol deposition, O'Riordan and Smaldone[19] studied upright humans with HIV under aerosolized pentamidine prophylactic therapy. The study focused on measuring the relationship between regional deposition and regional ventilation, and the influence of particle size and airway caliber on this relationship. The authors concluded that "differences in deposition between upper and lower lung regions are not accounted for simply by the differences in regional ventilation,"[19] which is not in agreement with our results.

However, there are several differences between the two studies that preclude a direct comparison, namely the measure of whole-lung deposition (deposition was only measured directly postaerosol inhalation in the study by O'Riordan and Smaldone[19]) versus alveolar deposition in our study, the population studied (HIV patients versus healthy subjects), posture (upright versus supine), particle size (0.8 and 2.5 μm versus 4.9 μm), and breathing pattern during aerosol inhalation (quiet tidal breathing versus controlled 1 L tidal breath at constant flow rate). Our previous work[8] has shown that deposition in the alveolar region is posture dependent, with 40% (seated) and 76% (supine) of particles depositing outside of the alveolar region. This observation together with the inclusion of tracheobronchial deposition may explain the different conclusions.

In a recent paper using a three-dimensional printed, realistic airway cast (mouth to generation 5), Verbanck et al.[40] reported for 3 and 6 μm particles, at higher flows than the flow imposed here (30 and 60 L/min, compared with 15 L/min), direct proportionality between lobar-level ventilation and aerosol distribution. The quartile lung regions used in our analysis samples ventilation and deposition across neighboring lobes. However, the scale of the analysis is of the order of lobar sampling (right lung). Therefore, the human data reported here support the cast data as well as the computational fluid dynamics (CFD) simulations presented in Ref.[40]

For scales smaller than the lobar level (segmental level), Verbanck et al. reported a higher variability in the cast's ventilation-to-deposition ratio. The limited lung coverage and co-registration across modalities (limitations given next) limit our ability to produce reliable data at the scale of lung segments and sub-segments. Our existing data at the regional lobar level are consistent across the seven subjects, potentially indicating the results obtained in a single realistic cast,[40] are robust and generalizable, at least for healthy individuals, despite the normal variance that is present in airway anatomy even between healthy individuals.

A recent work by Greenblatt et al.,[41,42] using similar-sized particles, compared the distribution of deposited particles with lobar-specific ventilation, using PET-CT, in asthmatics. Their work aimed at explaining and quantifying aspects determining inter-subject variability on peripheral particle deposition in asthmatics and concluded that differences in regional ventilation at a lobar level accounted for $\sim$1/3 (38%) of the variability in deposition,[42] with airway geometry at bifurcations and differences in deposition along the airway path accounting for the remaining $\sim$2/3 (38% and 31%, respectively).

The main difference between the work of Greenblatt et al. and the present study arise from the use of methacholine to induce bronchoconstriction; methacholine increases heterogeneity, resulting in a wider range of regional ventilation, and it is also likely to alter airway caliber and geometry. Moreover, that PET-CT study provided much broader lung coverage than our MRI-gamma scintigraphy study; lastly, the quantification of ventilation was inferred from either dynamic PET or static high resolution CT images comparing mid-lung volume with total lung capacity maneuver, whereas our technique operated in the more physiological tidal volume range.

Our data do not allow us to quantify the amount of variance explained by ventilation versus other potential causes, yet in accordance with Greenblatt et al.,[42] they support an important role for ventilation in the alveolar deposition of coarse particles in the supine human lung.

The main limitations of the approach described in this article were the partial lung coverage of the ventilation imaging and the co-registration step across the two imaging modalities. There were no fiduciary markers that allowed optimal alignment between the coronal projection image of deposition and the sagittal map of ventilation. Therefore, co-registration accuracy is limited. Specific ventilation imaging, as implemented here, provided only partial lung coverage, with a lung slice covering $\sim$8% of the lung volume. However, as the results and conclusions presented here refer to healthy subjects, a peripheral lung slice was likely representative of the response of the lung periphery as a whole, and, therefore, the limited sampling and co-registration uncertainty is unlikely to alter our results.

In disease, the heterogeneity of ventilation is higher,[43] and often localized regions of poor ventilation are present.[44–46] Importantly, if our findings are generalizable to the heterogeneous lung, the regions with lower ventilation—the areas that might be expected to benefit the most from inhaled topical action drugs—will be the ones that are less well targeted. For example, inhaled antibiotics in cystic fibrosis patients may fail to reach the affected periphery because of poor regional ventilation and instead likely be delivered mostly to regions of high ventilation, not where they may be the most effective and needed. This highlights the importance of alternate routes of drug delivery (systemic).

Depending on the target (proximal, peripheral airways), particle size, and drug pharmacokinetics, other factors such as second-pass effects of inhaled drugs, or, in case of reversible airway obstruction, the sequential combined use of bronchodilators, to improve regional ventilation to poorly ventilated regions, before inhaling the second drug may become actionable strategies. However, the relationship between regional ventilation and regional deposition is more complex and our findings may not hold in disease: For severe obstruction, depending on the degree of obstruction, the lower regional ventilation will be partly opposed by increased deposition efficiency within the airways from the reduced lumen radius, as well as increased flows and turbulence. The study by Brown et al.[18] included a group of cystic fibrosis patients who presented a more complex relationship between regional deposition and regional ventilation, with tracheobronchial deposition presenting a negative linear relationship, whereas parenchymal deposition was positively associated with regional ventilation.[18]

Lastly, the functional MRI ability to quantitatively discern fast equilibration in oxygen concentration (<1 breath), resulting from airways and/or potential regions of SV >1, is limited. The impact of this limitation is likely minor in the implementation described here, as the technique was applied to the peripheral lung, and the central region containing most of the large and intermediate airways was deliberately avoided, but will need to be addressed for accurate quantification of whole lung ventilation.

In conclusion, using an approach combining gamma scintigraphy and functional lung MRI, this study supports the hypothesis that for coarse particles ($\sim 5\,\mu$m), inhaled in the supine posture by subjects with a normal lung function, the fraction of regional deposition in the lung periphery (alveolar region) is directly proportional to the regional fraction of ventilation.

Acknowledgments

Contributions

R.C.S. and G.K.P. conceived the experiments, with significant input from C.D., K.L.Z., and W.D.B. R.C.S., K.L.Z., and W.D.B. performed the supine deposition and clearance data collection; R.C.S. and G.K.P. performed the MRI ventilation quantification. R.C.S. processed the MRI data, and K.L.Z. processed the clearance and deposition data. R.C.S. drafted the article and created the figures with C.D.'s help; all the co-authors contributed to the editing of the article, read and approved the final version.

Author Disclosure Statement

No competing financial interests exist.

References

1. Darquenne C: Aerosol deposition in health and disease. J Aerosol Med Pulm Drug Deliv 2012;25:140–147.
2. Mitchell DM, Solomon MA, Tolfree SE, Short M, and Spiro SG: Effect of particle size of bronchodilator aerosols on lung distribution and pulmonary function in patients with chronic asthma. Thorax 1987;42:457–461.
3. Usmani OS, Biddiscombe MF, and Barnes PJ: Regional lung deposition and bronchodilator response as a function of beta2-agonist particle size. Am J Respir Crit Care Med 2005;172:1497–1504.
4. Heyder J, Gebhart J, Rudolf G, and Schiller CF: Deposition of particles in the human respiratory tract in the size range 0.005–15 μm. J Aerosol Med 1986;17:811–825.
5. Laube BL, Janssens HM, de Jongh FHC, Devadason SG, Dhand R, Diot P, Everard ML, Horvath I, Navalesi P, Voshaar T, and Chrystyn H; European Respiratory Society; International Society for Aerosols in Medicine: What the pulmonary specialist should know about the new inhalation therapies. Eur Respir J 2011;37:1308–1331.
6. Darquenne C, Paiva M, and Prisk GK: Effect of gravity on aerosol dispersion and deposition in the human lung after periods of breath holding. J Appl Physiol 2000;89:1787–1792.
7. Bennett WD, Brown JS, Zeman KL, Hu S-C, Scheuch G, and Sommerer K: Targeting delivery of aerosols to different lung regions. J Aerosol Med 2002;15:179–188.
8. Sá RC, Zeman KL, Bennett WD, Prisk GK, and Darquenne C: Effect of posture on regional deposition of coarse particles in the healthy human lung. J Aerosol Med Pulm Drug Deliv 2015;28:423–431.
9. Montesantos S, Katz I, Fleming J, Majoral C, Pichelin M, Dubau C, Piednoir B, Conway J, Texereau J, and Caillibotte G: Airway morphology from high resolution computed tomography in healthy subjects and patients with moderate persistent asthma. Anat Rec (Hoboken) 2013;296:852–866.
10. O'Riordan TG, Walser L, and Smaldone GC: Changing patterns of aerosol deposition during methacholine bronchoprovocation. Chest 1993;103:1385–1389.
11. Richards R, Haas A, Simpson S, Britten A, Renwick A, and Holgate S: Effect of methacholine induced bronchoconstriction on the pulmonary distribution and plasma pharmacokinetics of inhaled sodium cromoglycate in subjects with normal and hyperreactive airways. Thorax 1988;43:611–616.
12. Hickey AJ: Back to the future: Inhaled drug products. J Pharm Sci 2013;102:1165–1172.
13. Lawrence M, Wolfe J, Webb DR, Chervinsky P, Kellerman D, Schaumberg JP, and Shah T: Efficacy of inhaled fluticasone propionate in asthma results from topical and not from systemic activity. Am J Respir Crit Care Med 2012;156:744–751.
14. Adcock IM, Gilbey T, Gelder CM, Chung KF, and Barnes PJ: Glucocorticoid receptor localization in normal and asthmatic lung. Am J Respir Crit Care Med 2012;154:771–782.
15. Laube BL: The expanding role of aerosols in systemic drug delivery, gene therapy, and vaccination. Respir Care 2005;50:1161–1176.
16. Laube BL: The expanding role of aerosols in systemic drug delivery, gene therapy and vaccination: An update. Transl Respir Med 2014;2:3.
17. Darquenne C, van Ertbruggen C, and Prisk GK: Convective flow dominates aerosol delivery to the lung segments. J Appl Physiol 2011;111:48–54.
18. Brown JS, Zeman KL, and Bennett WD: Regional deposition of coarse particles and ventilation distribution in healthy subjects and patients with cystic fibrosis. 2001;14:443–454.
19. O'Riordan TG, and Smaldone GC: Regional deposition and regional ventilation during inhalation of pentamidine. Chest 1994;105:396–401.
20. Darquenne C, Zeman KL, Sá RC, Cooper TK, Fine JM, Bennett WD, and Prisk GK: Removal of sedimentation decreases relative deposition of coarse particles in the lung periphery. J Appl Physiol 2013;115:546–555.
21. Bennett WD, Scheuch G, Zeman KL, Brown JS, Kim C, Heyder J, and Stahlhofen W: Bronchial airway deposition and retention of particles in inhaled boluses: Effect of anatomic dead space. J Appl Physiol 1998;85:685–694.
22. Bennett WD, Herbst M, Alexis NE, Zeman KL, Wu J, Hernandez ML, and Peden DB: Effect of inhaled dust mite allergen on regional particle deposition and mucociliary clearance in allergic asthmatics. Clin Exp Allergy 2011;41:1719–1728.

23. Lay JC, Berry CR, Kim CS, and Bennett WD: Retention of insoluble particles after local intrabronchial deposition in dogs. J Appl Physiol 1995;79:1921–1929.
24. Lee PS, Gerrity TR, Hass FJ, and Lourenco RV: A model for tracheobronchial clearance of inhaled particles in man and a comparison with data. IEEE Trans Biomed Eng 1979; 26:624–630.
25. Lippmann M, Yeates DB, and Albert RE: Deposition, retention, and clearance of inhaled particles. Br J Ind Med 1980;37:337–362.
26. Hofmann W, and Asgharian B: The effect of lung structure on mucociliary clearance and particle retention in human and rat lungs. Toxicol Sci. 2003;73:448–456.
27. Mortensen J, Lange P, Nyboe J, and Groth S: Lung mucociliary clearance. Eur J Nucl Med 1994;21:953–961.
28. Garrard CS, Mussatto DJ, and Lourenço RV: Lung mucociliary transport in asymptomatic asthma: Effects of inhaled histamine. J Lab Clin Med 1989;113:190–195.
29. Stahlhofen W, Gebhart J, and Heyder J: Experimental determination of the regional deposition of aerosol particles in the human respiratory tract. Am Ind Hyg Assoc J 1980;41: 385–398.
30. Zeman KL, Wu J, and Bennett WD: Targeting aerosolized drugs to the conducting airways using very large particles and extremely slow inhalations. J Aerosol Med Pulm Drug Deliv 2010;23:363–369.
31. Theilmann RJ, Arai TJ, Samiee A, Dubowitz DJ, Hopkins SR, Buxton RB, and Prisk GK: Quantitative MRI measurement of lung density must account for the change in $T(2)$ (*) with lung inflation. J Magn Reson Imaging 2009; 30:527–534.
32. Holverda S, Theilmann RJ, Sá RC, Arai TJ, Hall ET, Dubowitz DJ, and Prisk GK: Measuring lung water: Ex vivo validation of multi-image gradient echo MRI. J Magn Reson Imaging 2011;34:220–224.
33. Sá RC, Cronin MV, Cronin MV, Henderson AC, Holverda S, Theilmann RJ, Arai TJ, Dubowitz DJ, Buxton RB, and Prisk GK: Vertical distribution of specific ventilation in normal supine humans measured by oxygen-enhanced proton MRI. J Appl Physiol 2010;109:1950–1959.
34. Sá RC, Asadi AK, Theilmann RJ, Hopkins SR, Prisk GK, and Darquenne C: Validating the distribution of specific ventilation in healthy humans measured using proton MR imaging. J Appl Physiol 2014;116:1048–1056.
35. Arai TJ, Asadi AK, and Sá RC: *Deforminator: Projective Transformation to Register Small Scale Lung Deformation*. 1st ed. Github. hhttps://github.com/UCSDPulmonaryImaging/Deforminator (last viewing: Feb. 8, 2017).
36. Arai TJ, Villongco CT, Villongco MT, Hopkins SR, and Theilmann RJ: Affine transformation registers small scale lung deformation. Conf Proc IEEE Eng Med Biol Soc 2012; 2012:5298–5301.
37. Julien M, Flick MR, Hoeffel JM, and Murray JF: Accurate reference measurement for postmortem lung water. J Appl Physiol Respir Environ Exerc Physiol 1984;56:248–253.
38. Haeussermann S, Kietzig C, Sommerer K, and Usmani OS: Mode of breathing-tidal or slow and deep-through the I-neb Adaptive Aerosol Delivery (AAD) system affects lung deposition of 99m-Tc-DTPA. J Aerosol Med Pulm Drug Deliv 2010;23(S1):S37–S43.
39. Smaldone GC, Perry RJ, Bennett WD, Messina MS, Zwang J, and Ilowite J: Interpretation of ''24 hour lung retention'' in studies of mucociliary clearance. J Aerosol Med 1988;1:11–20.
40. Verbanck S, Ghorbaniasl G, Biddiscombe MF, Dragojlovic D, Ricks N, Lacor C, Ilsen B, de Mey J, Schuermans D, Underwood SR, Barnes PJ, Vincken W, and Usmani OS: Inhaled aerosol distribution in human airways: A scintigraphy-guided study in a 3D printed model. J Aerosol Med Pulm Drug Deliv 2016;29:525–533.
41. Greenblatt EE, Winkler T, Harris RS, Kelly VJ, Kone M, Katz I, Martin A, Caillibotte G, Hess DR, and Venegas JG: Regional ventilation and aerosol deposition with helium-oxygen in bronchoconstricted asthmatic lungs. J Aerosol Med Pulm Drug Deliv 2016;29:260–272.
42. Greenblatt EE, Winkler T, Harris RS, Kelly VJ, Kone M, Katz I, Martin AR, Caillibotte G, and Venegas J: What causes uneven aerosol deposition in the bronchoconstricted lung? A quantitative imaging study. J Aerosol Med Pulm Drug Deliv 2015;29:57–75.
43. Downie SR, Salome CM, Verbanck S, Thompson BR, Berend N, and King GG: Ventilation heterogeneity is a major determinant of airway hyperresponsiveness in asthma, independent of airway inflammation. Thorax 2007;62:684–689.
44. Venegas JG, Winkler T, Musch G, Vidal Melo MF, Layfield D, Tgavalekos N, Fischman AJ, Callahan RJ, Bellani G, and Harris RS: Self-organized patchiness in asthma as a prelude to catastrophic shifts. Nature 2005;434:777–782.
45. Altes TA, Powers PL, Knight Scott J, Rakes G, Platts Mills TAE, de Lange EE, Alford BA, Mugler JP, and Brookeman JR: Hyperpolarized 3He MR lung ventilation imaging in asthmatics: Preliminary findings. J Magn Reson Imaging 2001; 13:378–384.
46. Svenningsen S, Guo F, Kirby M, Choy S, Wheatley A, McCormack DG, and Parraga G: Pulmonary functional magnetic resonance imaging: Asthma temporal-spatial maps. Acad Radiol 2014;21:1402–1410.

Address correspondence to:
Rui Carlos Sá, PhD
Pulmonary Imaging Laboratory
Department of Medicine
University of California, San Diego
9500 Gilman Dr.
La Jolla, CA 92093-0852

E-mail: rcsa@ucsd.edu